BACHELOR

Flow development inside and behind a honeycomb measured with laser Doppler velocimetry

van der Lee, Koen J.M.

Award date:
2019

Department of Applied Physics
The Turbulence and Vortex Dynamics group
Bachelor End Project
BEP code: R-1975-B

Flow development inside and behind a honeycomb measured with laser Doppler velocimetry

K.J.M. van der Lee
Under supervision of R.A. Dellaert and J.C.H. Zeegers

Eindhoven, 12-07-2019

Abstract

This research focusses on the development of a flow inside and behind a honeycomb, which is investigated in different ways. The goal of this research is to get a better understanding of the flow development inside and behind the honeycomb, so that the efficiency of the MDS (magnetic density separator) can be increased. This development of the flow is investigated with measuring velocity profiles and the turbulence intensity profile. These velocity profiles are measured at different velocities and at different locations inside the wind tunnel, before being compared to the simulated velocity profiles. The turbulence intensity profile is measured in the Reynolds region where the transition from a laminar to a turbulent regime takes place, which gives a clear insight at which Reynolds number this transition takes place. The turbulence intensity profile is also compared to the values found in the paper written by Owolabi et al. [1].

Table of Contents

1. Introduction

Nowadays people are more and more concerned about the plastic pollution which fouls our planet. This plastic pollution can influence the ecosystems on land and in the sea; when plastics are dropped into the ocean, the plastic breaks down in so called micro plastics, which are toxic for sea life [2]. Plastic pollution which is eliminated with the use of combustion also contributed to the greenhouse effect, because carbon dioxide gasses are released during this process. There is so much plastic nowadays, that plastic has even been detected at the deepest point on the earth, the Mariana Trench [3]. To overcome the problem of the increasing plastic pollution and the combustion of plastic pollution, plastic needs to be recycled. A promising idea in the field of plastic recycling is the MDS (magnetic density separator), which separates plastics according to their different mass densities.

To recycle plastic pollution, it has to be separated in different mass densities in order to make the recycled plastic useful again. Nowadays, plastic pollution consists of different types of plastic, which each have a different mass density. When this plastic pollution is recycled, the recycled plastic is impure, due to the different mass densities. This asks for a way to separate the plastic on a mass density basis. A MDS (magnetic density separator) machine is used to realize this mass density specific sorting . A picture of this separator is shown in figure 1.

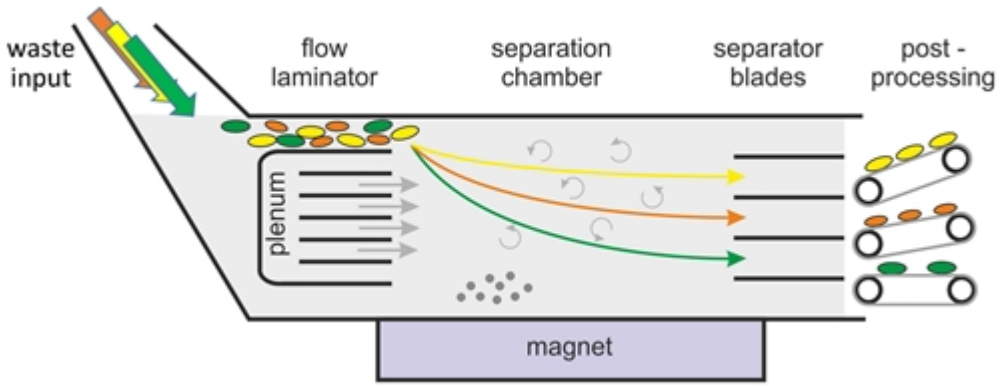

Figure 1 : Schematic overview of the magnetic density separator (MDS) [4].

At the left top of the MDS are plastic flakes entering the separator. These plastic flakes are about $10\ mm$ in size and are submerged into a ferrofluid. Due to the magnet and the ferrofluid, the plastic flakes experience an attracting force (effective mass density field) which is directed towards the magnet. This force makes sure that the flakes with different mass densities experience different forces towards the magnet. This makes the separation of the flakes on the base of their mass density possible. When the flakes are separated, they are collected in the separator blades. At the end of the separator blades is the post processing process, where the plastics with different mass densities are collected and transported away.

It is important to have a flow profile in the separation chamber which has a turbulence level as low as possible, otherwise the plastic flakes tend to mix with each other. This is the reason why there is a flow laminator used in the MDS machine. This laminator creates laminar flow profiles at the end of each plenum tube. The separation walls between the different flows can create turbulent vortices, which contribute to a turbulent flow. These separation walls can be big (walls between flow laminator and upper or lower flow) or small (walls between flow laminator flows).
In the separation chamber, the upper, lower and plenum flows recombine to one flow profile.
For a good MDS machine, the turbulence level must be as low as possible in the separation chamber in order to reach the optimal recycling efficiency.

During this project, the flow in the separation chamber is studied in a wind tunnel. This wind tunnel is made, such that the circumstances are similar in the wind tunnel as in the separation chamber of the MDS. This similarity of circumstances is made possible, because the Reynolds numbers inside the MDS machine are the same as those inside the wind tunnel. The flow laminator that is used in this research is a so called honeycomb. This honeycomb is a tube bundle consisting of small rectangular pipes.

This report describes the flow properties inside the separation chamber of the MDS and at the end of the plenum tubes and compares those with the values according to the theory and a paper.

In chapter 2, the theory of fluid dynamics will be discussed, which makes it possible to understand the results of the research. Chapter 3 discusses the experimental setup, which made it possible to do all the measurements. In chapter 4, the results of this research are discussed, which are displayed in tables and/or figures. Chapter 5 contains the conclusion and the discussion, which contains a summary of the results and suggests some options to improve measurements in further research. Chapter 6, at last, consists of the suggestions for further research.

2. Theory

In this chapter, the background theory of fluid dynamics will be discussed. This will be used in this research to work out the results and to compare different results with each other. The research for this project was done in a wind tunnel where the flow exists out of pure nitrogen gas. The flow in the wind tunnel is similar to the flow in the MDS machine, because the Reynolds similarity was applied. In section 2.1, the Navier-Stokes equations will be explained. Those equations are the most important equations in the field of fluid dynamics, because they can be used to calculate all the flow properties. Section 2.2 contains all the theory which is used to explain and compare the results of the measured flow. In section 2.3, different topics will be discussed, which could cause instabilities in the flow. At last, a comparison will be made between the velocities inside the wind tunnel and the MDS machine. This comparison is made and worked out in section 2.4

2.1 Navier-Stokes equations

The equation that is the backbone for all the fluid and gas dynamics is the Navier-Stokes equation. Almost all the flow properties can be derived from the Navier-Stokes equation. The equation is a nonlinear partial differential equation. The Navier-Stokes equation for incompressible Newtonian fluids is shown in equation (2.1)

$$\rho \frac{\partial \boldsymbol{v}}{\partial t} + \rho(\boldsymbol{v} \cdot \nabla)\boldsymbol{v} = -\nabla p + \mu \nabla^2 \boldsymbol{v} + \boldsymbol{f} \tag{2.1}$$

where ρ is the density in $kg \cdot m^{-3}$, $\boldsymbol{v}$ is the velocity vector in $m \cdot s^{-1}$, μ is the dynamic viscosity in $\mathrm{kg} \cdot \mathrm{m}^{-1} \cdot s^{-1}$ and $\boldsymbol{f}$ is the force vector that acts on the fluid inside the flow. There is also a differential equation which describes the conservation of mass during the flow, which is shown below in equation (2.2).

$$\frac{\partial \rho}{\partial t} + \nabla \cdot (\rho \boldsymbol{v}) = 0 \tag{2.2}$$

For an incompressible fluid or a gas far below the speed of sound, the density ρ is constant, which means that the equation for the conservation of mass can be reduced to $\nabla \cdot \boldsymbol{v} = 0$.

2.2.1 Reynolds number

The Reynolds number (*Re*) is the most important dimensionless number for this research.
The number is the ratio between the inertial forces and viscous forces in the flow. A high Reynolds number indicates that the inertial forces are dominant and a low Reynolds number indicates that the viscous forces are dominant in the flow.
The Reynolds number is also used to predict flow patterns in different fluid flow situations. The formula that describes the *Re*, is given by equation (2.3)

$$Re = \frac{UL}{\nu} = \frac{UL\rho}{\mu} \tag{2.3}$$

where U is the mean velocity of the flow in $m \cdot s^{-1}$, L is the characteristic length scale of the object in m and ν is the kinematic viscosity in $m^2 \cdot s^{-1}$. The value of L is equal to the diameter (D), considering a circular pipe flow. The dynamic viscosity ($\mathrm{kg} \cdot \mathrm{m}^{-1} \cdot s^{-1}$) is related to the kinematic viscosity in the following way: $\nu = \mu/\rho$, where ρ is the density of the fluid in $kg \cdot m^{-3}$.
According to the literature [5], a pipe flow has different properties at different Reynolds numbers. The properties of the pipe flow at a certain Reynolds number are shown in table 1.

Table 1 : Reynolds numbers at which a pipe flow is laminar, in the transition zone and turbulent.

$Re < 2300$	$2300 < Re < 4000$	$Re > 4000$
Laminar flow	*Transition zone*	*Turbulent flow*

Despite the fact that the Reynolds numbers from above apply to circular pipe flows, they should give the same results as the square duct flow from this research.

2.2.2 Hydraulic diameter

When there is a flow inside a circular pipe, the value of L is equal to the diameter of the pipe. During this research, the flow flows through approximately rectangular cross sections. In this case, the value of L is described with the value D_h, which is called the hydraulic diameter. The hydraulic diameter is described by equation (2.4)

$$D_h = \frac{4A}{P} = \frac{2hw}{h+w} \tag{2.4}$$

where A is the cross sectional area of the pipe in m^2, P is the wetted parameter, which is equal to $2h + 2w$, w is the width of the channel in m and h is the height of the channel in m.

2.2.3 Viscosity

In order to calculate the Reynolds number, different types of viscosity could be used. The relation between the kinematic and dynamic viscosity is $\mu = \rho \cdot \nu$, as described in the previous section. The dynamic viscosity is temperature dependent, according to the Arrhenius model [6]. The formula is shown below

$$\mu(T) = \mu_0 \exp\left(\frac{E}{RT}\right) \tag{2.5}$$

where μ_0 is a coefficient, E is the activation energy in J, R is the universal gas constant in $J \cdot K^{-1} \cdot mol^{-1}$ and T is the temperature in Kelvin (K).
The gas that is used during this research is nitrogen. The value of E for nitrogen is constant, so μ only depends on T.
The experiments during this research were done around room temperature ($293K$) and at atmospheric pressure $1\ atm$. The values of ρ and μ at this temperature are $1.165\ kg \cdot m^{-3}$ [7] and $1.76 * 10^{-5}\ Pa \cdot s$ [8].

2.2.4 Hydrodynamic entrance length

A flow is fully developed when the average velocity profile does not change anymore as a function of distance downstream. This means that the flow profile will remain the same. The distance a flow needs to become fully developed is called the hydrodynamic entrance length. The entrance lengths for fully laminar and turbulent flows are different. For the laminar flow, the entrance length can be calculated with equation (2.6) [9].

$$L_{h,laminar} = 0.05 R_e D_h \tag{2.6}$$

The hydrodynamic entrance length for a turbulent flow is given in equation (2.7)

$$L_{h,turbulent} = 4.4 D_h (R_e)^{1/6} \tag{2.7}$$

where L_h is the laminar or the turbulent hydrodynamic entrance length in m and D_h is the hydraulic diameter in m.

The velocity profiles of the laminar and turbulent profiles look different. The laminar and turbulent flow profiles are shown in figure 2.

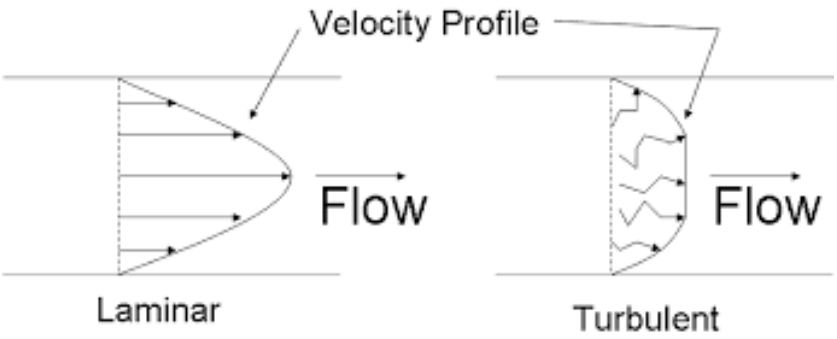

Figure 2 : A parabolic (laminar) flow profile on the left and a turbulent flow profile on the right [10].

The laminar flow profile has a parabolic shape and the turbulent flow profile has a more flattened shape. The laminar flow profile emerges at low Reynolds numbers $Re < 2300$ and the turbulent flow profile emerges at high Reynolds numbers $Re > 4000$ [11]. The different flow patterns can be explained with the use of the Reynolds number. In both profiles, the velocity at the wall is 0 due to the no slip condition. In the laminar case, the viscous forces are dominant, which influences the flow at the walls. This gives rise to a laminar boundary layer. Due to the mass conservation, the flow in the middle will have a higher velocity than the velocity near the walls, because the flow in the middle is less affected by the viscous forces. In the turbulent case, the viscous forces are small, which implies that the flow is less affected by the viscous forces. This explains why the flow pattern of the turbulent flow profile is more flattened.

2.2.5 Turbulence intensity

In the field of fluid dynamics, the turbulence intensity is an important number. It describes how turbulent the flow is at a given point. The formula for the turbulence intensity is shown in equation (2.8) [12]

$$I = \frac{v_{RMS}}{v_{mean}} * 100 \tag{2.8}$$

where I is the turbulence intensity in $\%$, v_{RMS} the RMS value of the velocity fluctuations in $m \cdot s^{-1}$ and v_{mean} the mean velocity in $m \cdot s^{-1}$. The v_{RMS} is the RMS value of the total velocity, which means that the v_{RMS} can be composed from the RMS values in each direction. This is shown in equation (2.9)

$$v_{RMS} = \sqrt{\frac{1}{3}\left(v_{RMSx}^2 + v_{RMSy}^2 + v_{RMSz}^2\right)} = \sqrt{\frac{2}{3}k} \tag{2.9}$$

where v_{RMSi} is the RMS value of the velocity in an arbitrary direction in $m \cdot s^{-1}$ and k is the so-called turbulent energy in $(m \cdot s^{-1})^2$.
The value of v_{mean} is the total mean velocity, which means that v_{mean} can be composed in the average velocities in each direction, which is shown in equation (2.10).

$$v_{mean} = \sqrt{v_{meanx}^2 + v_{meany}^2 + v_{meanz}^2} \quad (2.10)$$

2.3.1 Kelvin-Helmholtz instability

The Kelvin-Helmholtz instability can occur when there is a velocity difference between two fluid layers. The instability separates the fluid into two layers, but the discontinuity occurs in the middle of the two layers. This discontinuity in the tangential velocity induces vorticity at the interface. Due to this vorticity, the interface becomes an unstable vortex sheet [13]. An example of a Kelvin-Helmholtz instability is the creation of vortices when two layers of air meet with each other, which is illustrated in figure 3.

Figure 3 : Example of a Kelvin-Helmholtz instability [14].

During experiments, a Kelvin-Helmholtz instability can also occur when the flows from different channels recombine with each other, because the flows in each channel have slightly different velocity components.

2.3.2 Karman vortex street

In the field of fluid dynamics, a Karman vortex street is a repeating pattern of vortices, caused by a process which is called vortex shedding. This vortex shedding is responsible for the creation of vortices in a flow around blunt bodies. A schematic representation of a Karman vortex street is shown in figure 4.

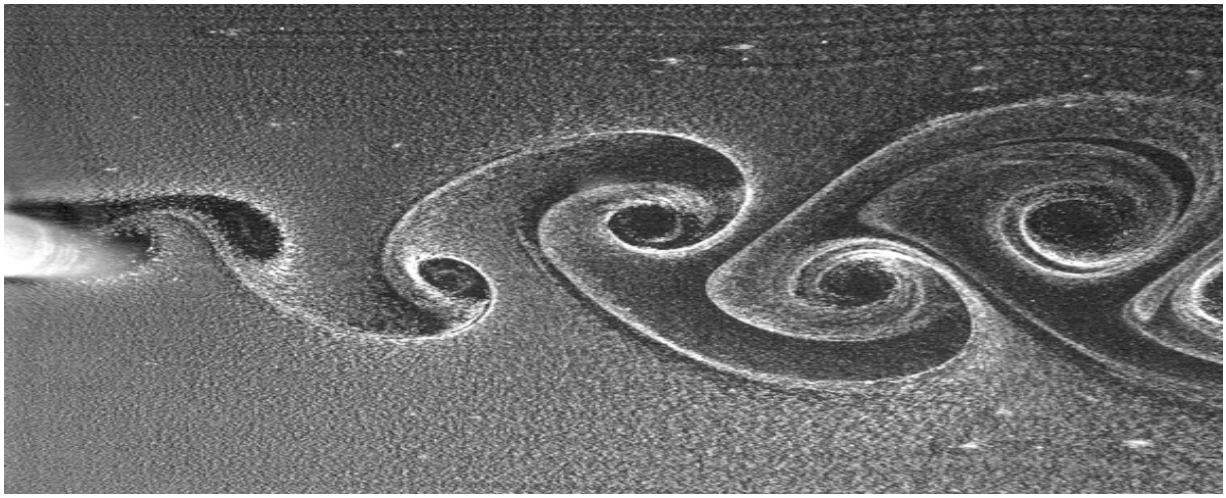

Figure 4 : Karman vortex street behind a sphere [15].

A vortex street will only occur at certain flow velocities (Reynolds numbers). A fluid can only create a vortex street when $Re > 90$ [15].
During this experiment, Karman vortex streets can occur behind the small honeycomb channel separation walls and the channel separation walls. The vortices behind the two channel separation walls will be larger than the vortices behind the thin honeycomb channel separation walls, because of the different thicknesses of the separation walls.
These vortices combined with the Kelvin-Helmholtz instabilities can create interesting flow profiles and can be used to explain those flow profiles.

2.4 Comparison to the MDS

The wind tunnel which is used during this research is a scaled down version of the MDS. This means that the Reynolds number inside this wind tunnel is exactly the same as in the MDS. With that information, it is possible to calculate the velocity inside the MDS, for a given value of the velocity inside the wind tunnel. How this can be done, is shown in equation (2.11)

$$v_{MDS} = v_{exp} \frac{D_{h,exp}}{D_{h,MDS}} \frac{\rho}{\rho_{MDS}} \frac{\mu_{MDS}}{\mu} \qquad (2.11)$$

where v_{MDS} is the velocity in the MDS in $m \cdot s^{-1}$, $D_{h,MDS}$ is the hydraulic diameter of the MDS in m, ρ_{MDS} is the density of the ferrofluid used in the MDS in $kg \cdot m^{-3}$ and μ_{MDS} is the dynamic viscosity of the ferrofluid in the MDS in $Pa \cdot s$.
To give a clear overview, the constants of equation (2.11) are shown in table 2, in which the constants for this research are based on nitrogen in gas form.

Table 2 : Constants during this research and constants in the MDS.

ρ	ρ_{MDS}	μ_{MDS}	μ
$1.165\ kg \cdot m^{-3}$	$1008\ kg \cdot m^{-3}$	$0.00105\ Pa \cdot s$	$1.76 \cdot 10^{-5}\ Pa \cdot s$

The values of $D_{h,exp}$ and $D_{h,MDS}$ depend on what parts of the wind tunnel and the MDS are being compared with each other. In this section, the velocities in both channels downstream the honeycomb and the velocities in both honeycomb channels are compared with each other and written as a function of v_{MDS} and v_{exp}, where v_{MDS} is the mean velocity inside a MDS section ($m \cdot s^{-1}$) and v_{exp} is the mean velocity inside a wind tunnel section ($m \cdot s^{-1}$).

The channel behind the honeycomb in the wind tunnel and the channel behind the honeycomb in the MDS

The values of $D_{h,expch}$ and $D_{h,MDSch}$ are $74.4\ mm$ and $169.8\ mm$. This gives the following relation between the v_{expch} and v_{MDSch}

$$v_{expch} = 33.1 \cdot v_{MDSch} \qquad (2.12)$$

The honeycomb channel in the wind tunnel and the honeycomb channel in the MDS

The values of $D_{h,exphc}$ and $D_{h,MDShc}$ are $9.45\ mm$ and $3.75\ mm$. This gives the following relation between the v_{exphc} and v_{MDShc}

$$v_{exphc} = 5.75 \cdot\ v_{MDShc} \qquad (2.13)$$

Experimental Setup

In this chapter, the experimental setup will be discussed. An overview of the lab can be seen in figure 5, where all the parts of the lab are shown. The general parts of the lab, which do not need any deep explanation, are discussed in section 3.1. The most important parts of the lab and for this research were the lasers, the wind tunnel, the humidifiers and the honeycomb. Those will be discussed separately in part 3.2. These parts will also be explained in more detail than the other parts.

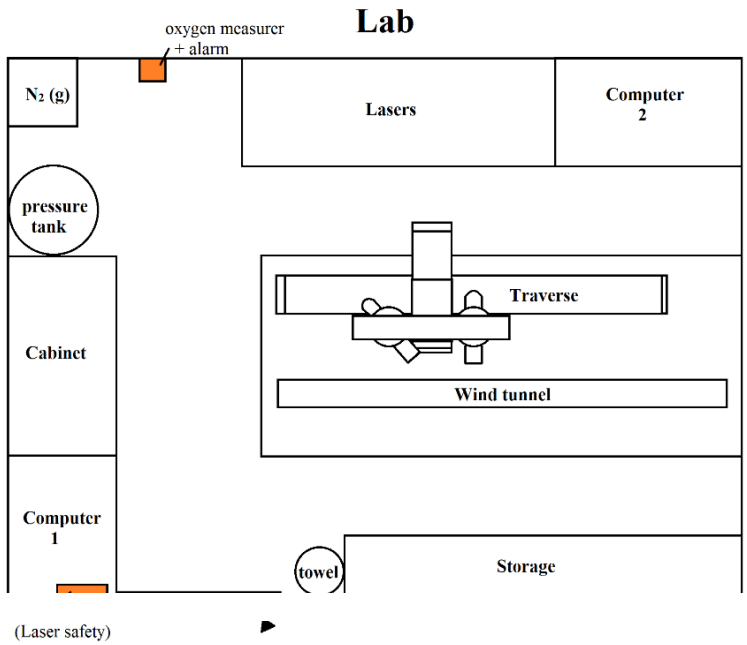

Figure 5 : Schematic top view of the lab [17].

3.1 Computers, cabinet and pressure tank

Computer 1 contains the system which regulates the flow. This computer regulates the humidity, velocity and pressure. The humidity can be set in the top/bottom and middle channel separately, while the velocity can be set in each channel separately. The desired velocity that is put into the software is called the set velocity. The software of computer 1 is connected to the cabinet, where the most important parts are to generate the flow. The cabinet contains the water for the humidifiers, many cables, pipes and three different valves for creating the desired velocity.
Those valves are used for the flow and velocity control in the wind tunnel. There is a small, medium and big valve. The small valve is used at low set velocities and the medium valve is used at higher set velocities. The big valve opens at a set velocity of $4.9\ m \cdot s^{-1}$ in the middle channel. However, the set velocity of $4.9\ m \cdot s^{-1}$ was never reached during this research, so the big valve is not used. At a set velocity of $1.0\ m \cdot s^{-1}$ in the middle channel, changes the small valve to the medium valve. Above a set velocity of $1.0\ m \cdot s^{-1}$ in the middle channel is the medium valve used for creating the flow. The percentage of opening of the medium valve is determined by the set velocity and the pressure. At higher pressures is the percentage of opening lower than at low pressures, considering the same velocity. The medium valve functions optimal when this percentage is between 20 and 80 percent, which was always the case during this research. For creating the velocities in the upper and lower channel, only the small valves were needed, because the cross sectional areas of those channels are 5 times smaller compared to the middle channel.
Computer 2 contains the software for the lasers and the traverse. With the use of the lasers, it is possible to calculate the different velocities inside the flow. More information about the laser and the measurement technique will be explained further on. With the software of the traverse, it is

possible to move the laser in three different directions. The software also contains pre-written scripts, which made it possible for the laser to do full-automatic measurements.
The cables in the cabinet are used for the connection between the water reservoir and the humidifiers. Pipes make sure that the created flow will go from the cabinet through the humidifiers, before going through the wind tunnel. The humidifiers lay on top of the wind tunnel and add water droplets to the nitrogen flow. One humidifier regulates the humidity in the middle channel, while the two other humidifiers regulate the humidity in the top and bottom channel. More about the humidifiers will be explained in section 3.3.4.
The pressure is regulated by a pressure regulator and pressure tank, which dampens flow variations down to below 1%. Higher pressure is needed for higher velocities, but there is a limit to the velocity inside the wind tunnel; the flexible pipes, which connect the pressure tank with the cabinet, can only handle a pressure up to $5\ Bar$.

3.2.1 Wind tunnel

The experiments of this research are done in the wind tunnel. The wind tunnel is connected with the humidifier and with the cabinet though 3 supply pipes. A schematic figure of the wind tunnel is shown in figure 6.

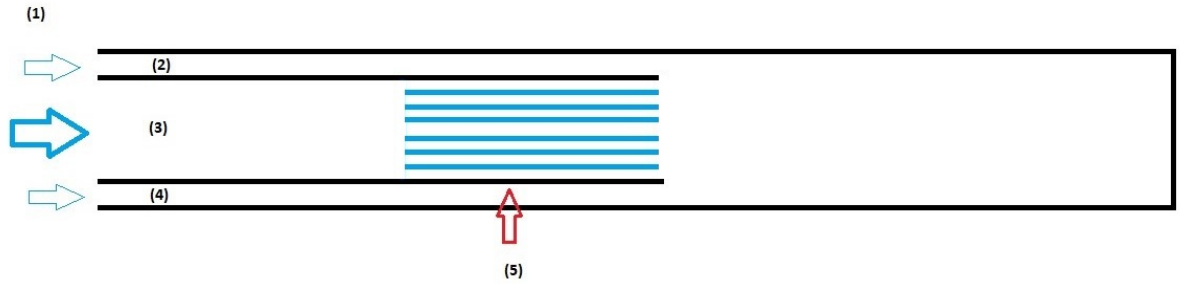

Figure 6 : Schematic cross section of the wind tunnel where (1) consists of 3 arrows which each represent a pipe flow corresponding to a certain channel, (2) is channel 1 (top), (3) is channel 2 (middle), (4) is channel 3 (bottom) and (5) is the honeycomb.

Figure 6 shows that the flow is entering the wind tunnel in three different channels. Those three channels are separately connected with the humidifier through pipes. This makes it possible to set the humidity of the middle channel and the upper plus lower channel separately. The upper channel is numbered with number 2, the middle channel is numbered with number 3 and the lower channel is numbered with number 4. The velocity can be set in each of these channels individually, but during this research all velocities in the individual channels are kept the same. Number 5 is the honeycomb, which consists of 35 almost squared pipes. At the end of the honeycomb, the flows of the honeycomb channels combine with the flows of channel 1 and 3. More about the honeycomb will be explained in section (3.2.2). The dimensions of the wind tunnel are shown in table 3.

Table 3 : Dimensions of the wind tunnel.

Length	Full width	Full height
$\pm\ 3000\ mm$	$70\ mm$	$80\ mm$

Figure 7 shows a side view of the wind tunnel with its length.

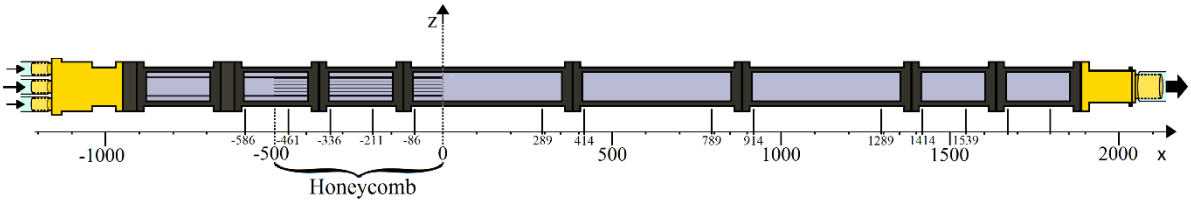

Figure 7 : Side view of the wind tunnel.

The honeycomb is located at $1000\ mm$ behind the flow entrance, which means that the flow can be measured up to $2000\ mm$ behind the honeycomb. The dimensions of the cross section of the wind tunnel are shown in figure 8.

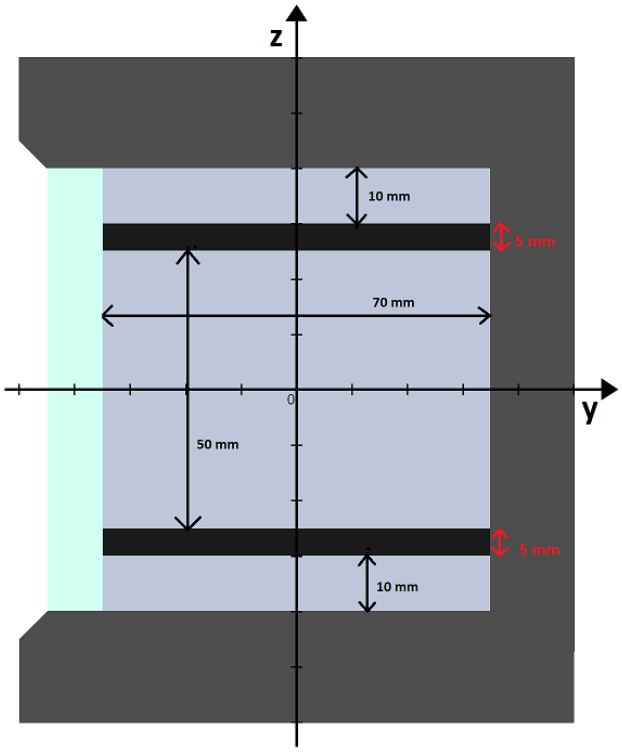

Figure 8 : Cross sectional image of the wind tunnel.

The velocities in channel 1, 2 and 3 upstream of the honeycomb are equal to the set velocities of each channel. The velocities inside the honeycomb channels and behind the honeycomb are not equal to the set velocity, because of the different cross sectional areas through which the flow flows. Considering the constant mass flow leaves the following relations between the set velocities v_{set} and the mean velocities inside a honeycomb channel v_{meanhc} and downstream the honeycomb v_{meanch}. The relations which involve v_{meanhc} during this research are based on the mean velocity inside a honeycomb channel of the honeycomb which is used during this research. This means that this value does not hold for other honeycombs.

$$v_{set} = 0.893\ v_{meanhc} \tag{3.1}$$

$$v_{set} = \frac{8}{7}\ v_{meanch} \tag{3.2}$$

The Reynolds numbers are not everywhere the same inside the wind tunnel, because of the different hydraulic diameters at different locations. Table 4 shows the different Reynolds numbers inside the honeycomb and downstream of the honeycomb for different v_{set} values.

Table 4 : Reynolds numbers (honeycomb channel and channel downstream of the honeycomb) for different set velocities.

$v_{set}\ (m \cdot s^{-1})$	Re_{hc}	Re_{ch}
0.1	70	432
1.0	701	4325
2.0	1401	8649
3.0	2102	12974

3.2.2 Honeycomb

The honeycomb that is used during this research is the type HC50Gc (Appendix). All the measurements during this research are done with the same honeycomb inside the wind tunnel. The dimensions of the honeycomb are shown in figure 9.

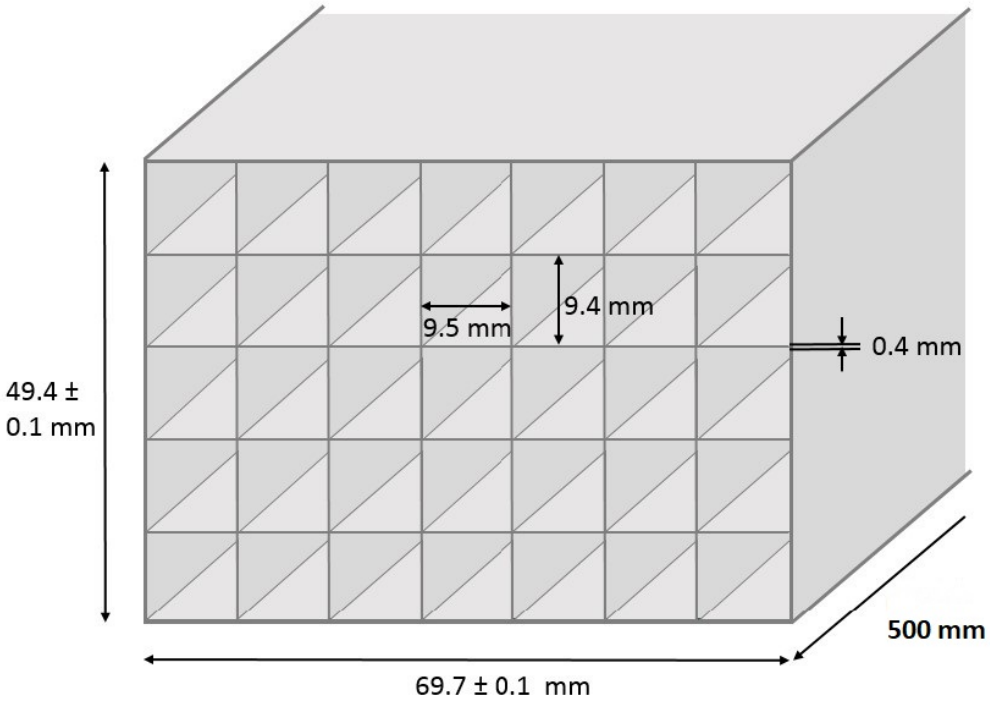

Figure 9 : Cross sectional mage of honeycomb HC50Gc.

The height of the honeycomb is $49.4\ \pm 0.1\ mm$ and the width is $69.7\ \pm 0.1\ mm$. The honeycomb channels are 9.5 by $9.4\ mm$, which gives them a value of $D_{hhc} = 9.45\ mm$. The thickness of the walls is $0.4\ mm$, which creates the smaller flow area. The honeycomb fits exactly into the middle channel, which means that there is no flow loss around the outer walls of the honeycomb. It is possible to calculate the entrance lengths for turbulent and laminar flows inside a honeycomb channel, but for this research are only the laminar entrance lengths inside the honeycomb important, which are shown in table 5 for different v_{set} values.

Table 5: Laminar entrance length inside a honeycomb channel for different Reynolds numbers

$v_{set}\ (m \cdot s^{-1})$	$L_{hlam}\ (m)$
0.1	0.033
1.0	0.33
2.0	0.66
3.0	0.99

The honeycomb is $500\ mm$ long, which means that not all the flow patterns will be fully laminar at the end of the honeycomb channels.

3.2.3 Laser

With the use of Laser Doppler Velocimetry (LDV), it is possible to do accurate point-measurements on the flow inside the wind tunnel. LDV is an optical measurement technique, which is also used during this research. In the lab, a full 3D TSI laser Doppler velocimeter is used. A schematic overview of the principle of a LDV setup is shown in figure 10.

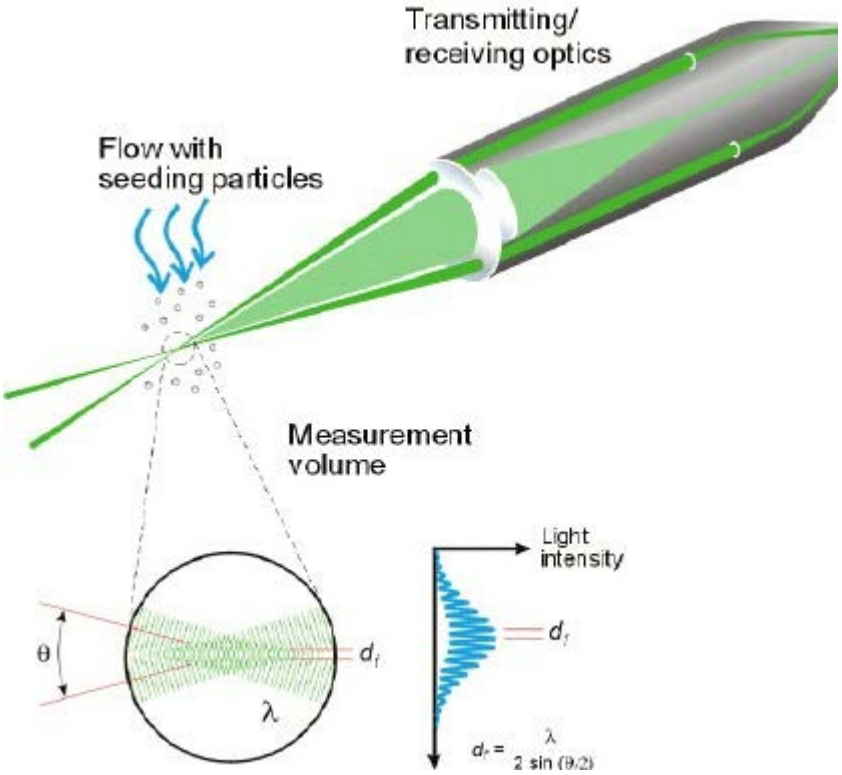

Figure 10 : LDF setup [16].

LDV is based on two or more laser beams which intersect with each other at an angle θ. The probe volume, also called measurement volume, is the place where the two laser beams will intersect. The probe volume is typically a few mm long. At this place, the light intensity is modulated due to the interference between the laser beams. Due to this interference, places of low and high light intensity will emerge, so called fringes. The fringe distance can be described with equation (3.3) [16]

$$d_f = \frac{\lambda}{2 \cdot Sin(\frac{\theta}{2})} \tag{3.3}$$

where d_f is the fringe spacing in nm, λ is the wavelength of the laser light in nm and θ is the angle between the two laser beams.

Each particle scatters light proportional to the local intensity. The velocity information of the flow comes from the light that is scattered by the water droplet, when it crosses the probe volume. The scattered light contains a Doppler shift with a so called Doppler frequency (f_d). This Doppler frequency is proportional to the velocity component perpendicular to the bisector of the two laser beams $f_d \sim U_\perp$.
When the scattered light is collected by a receiver lens, it is focused on a photo-detector. The photo detector makes sure that only the required wavelength passes to the photo-detector. The remaining wavelengths are filtered out by an interference filter.

The photo-detector converts the fluctuating light intensity to an electrical signal, which is called the Doppler burst. Those Doppler bursts are filtered and amplified in the signal processor. This signal processor determines the f_d for each particle. The fringe spacing, d_f, provides information about the distance traveled by the particle and the Doppler frequency f_d provides information about the time needed to cover d_f. The expression for the velocity is then $U_\perp = d_f \cdot f_d$.
Due to the constant frequency shift between the two lasers, the fringes move at a constant velocity. Particles which are not moving will generate a signal of this frequency shift, which is shown in figure 11.

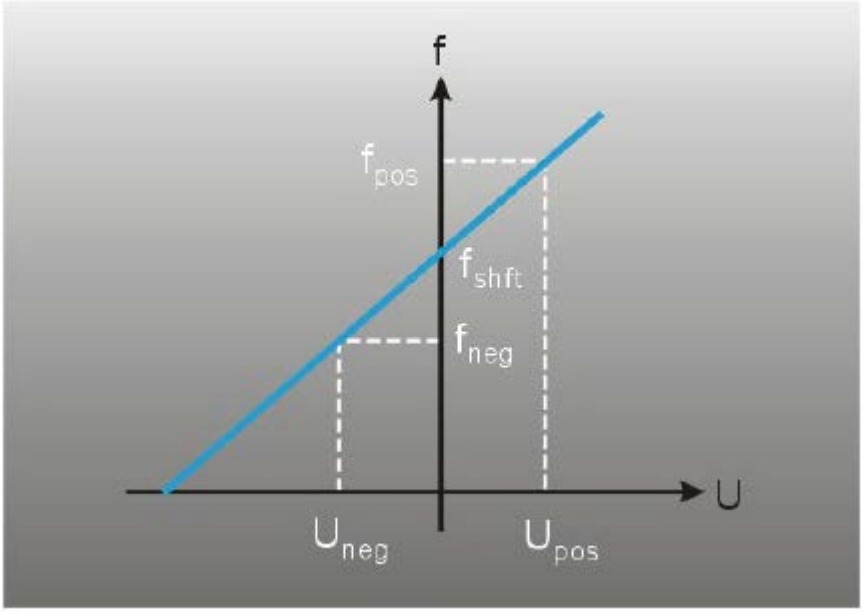

Figure 11: Doppler frequency to velocity [16].

It can be seen that Doppler frequencies lower than the constant frequency shift are measured for particles that move in the negative direction. This makes it possible for the LDV to measure the velocity of the water droplets and to indicate if their velocity is positive or negative.
In order to measure two velocity components, two extra beams can be added in a plane perpendicular to the two first two beams.
During this research, all the three velocity components of the water droplet are measured. This can be done with the setup, which is shown in figure 12.

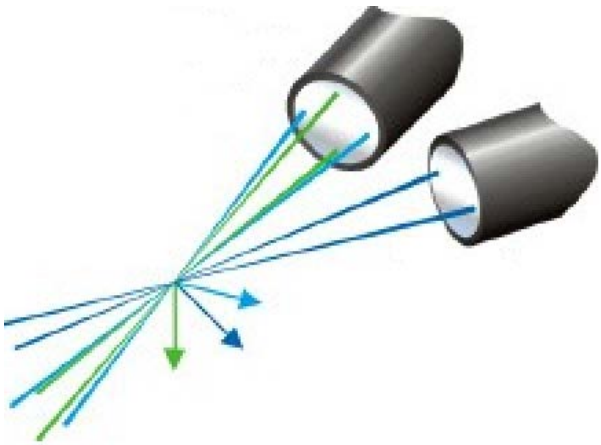

Figure 12 : Laser setup for measuring 3 velocity components [16].

All the 6 beams are intersecting in the same point, where the velocity is measured in the same way as for the one dimensional case. Each laser couple has a different wavelength, so that the components can be distinguished between each other. There are also three photo-detectors needed with the appropriate interference filters in order to detect the scattered light of the three wavelengths.

3.2.4 Humidifiers

The experimental setup contains three humidifiers; two for regulating the amount of tracer particles in the top and bottom channel and the other one for regulating the tracer particles in the middle channel. The humidifiers are made by UCAN systems consisting of 4 or 8 TDK ultrasonic nebulizers, which turn the water into water droplets. The two humidifiers in the top and bottom channels are the same and a schematic side view of such a humidifier is shown in figure 13. The humidifier installed in the middle channel looks similar to the humidifiers of the top and bottom channel but has a higher capacity and a wider channel.

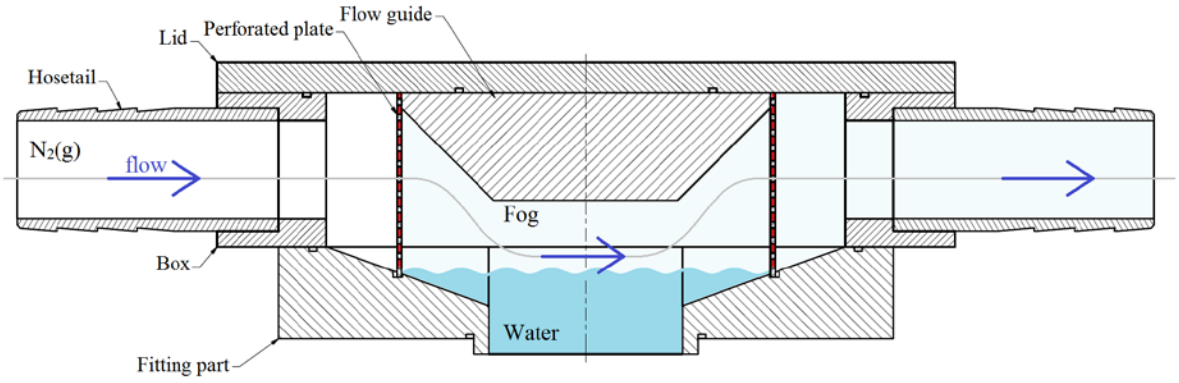

Figure 13 : Cross sectional view of a top/bot humidifier [17].

The humidifiers have been adapted in order to have a closed off flow over the water bath in the UCAN unit. The generated fog is taken up by the nitrogen flow and evaporates until a humidity of 100% is reached. When a humidity of 100% is reached, the water droplets in the fog taken up by the nitrogen flow act as tracer particles.
Those tracer particles make it possible to de measurements on the flow with the use of LDV.
The humidity of the humidifier can be set manually in the program of computer 1, where the humidity of the upper and lower channels are the same. The set humidity represents the scale at

which rate the humidifier turns water into fog, which is not the same as the real humidity of the flow.
The humidifiers work properly up to a certain temperature. When the water in the water reservoir reaches $31\ °C$, the humidifiers stop working and the data rate drops. This was only a problem at low velocities. To fix this problem, ice was added to the reservoir water, which kept the humidifiers cool during those measurements.

4. Results

In this chapter, the results from this research will be shown. The results are used for a better understanding of the flow behavior inside the wind tunnel and will be shown in a chronological order. When needed, pictures about the location of the measurements are added. Those pictures give a clear indication of where the measurements were taken.

4.1 Humidity check

The data rate inside the wind tunnel is the amount of measurements the LDV does per second. The data rate during the measurements is a function of the concentration of tracer particles inside the wind tunnel, which can be controlled by the humidifiers. Getting a high data rate is recommended, however this can create a problem. When the concentration of tracer particles, which exist out of small water droplets, is very high, condensation against the walls of the wind tunnel starts to occur. This condensation will start to flood the wind tunnel during the experiments and can affect the flow and therefore the results. So, a balance has to be found in having an as high as possible data rate without flooding the wind tunnel. An experiment for this has been setup were we measured the minimal set humidity while still getting a data rate. This minimal set humidity was the lowest set humidity value, where the laser still diffracts onto the passing water droplets. The data rate, which is proportional to the concentration of tracer particles, remains the same during the whole experiment. The results of this experiment can later be used as guideline for further experiments. The relation between the minimal humidity values and the set velocity is shown in figure 14.

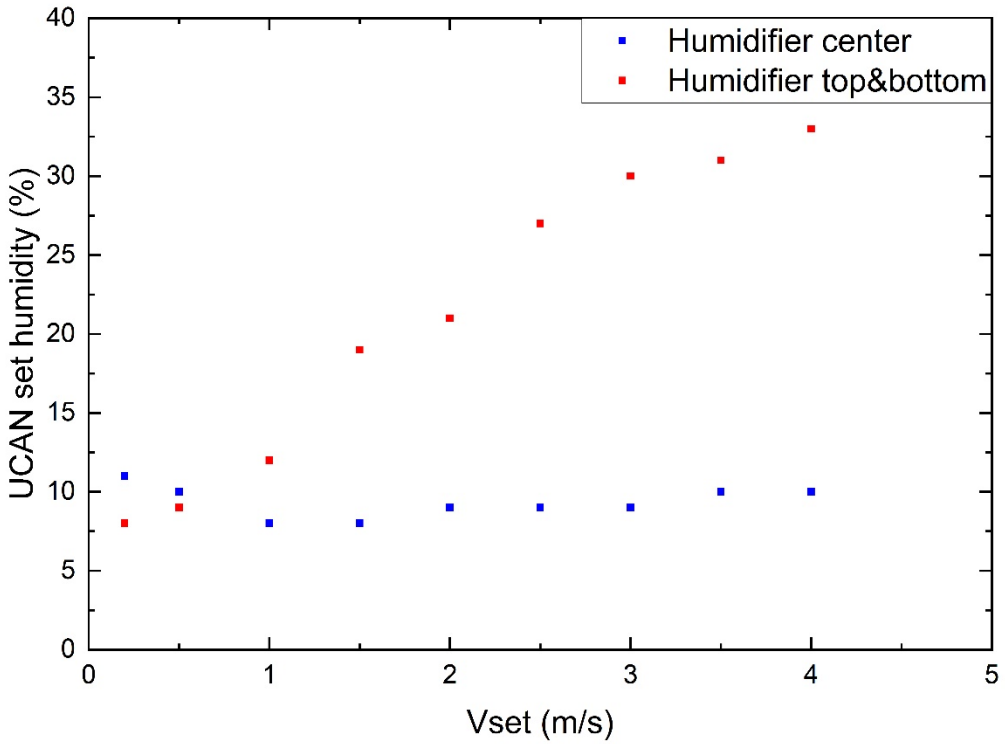

Figure 14 : Minimal set humidity of the humidifier as a function of v_{set}.

It can be seen that the relation between the set humidity of the humidifier and the set velocity is different for the humidifier in the top/bot channel than in the middle channel. The reason for this are the different shapes and capacities of the humidifiers. The humidifier for the middle channel has a higher capacity and width according to section 3.3.4. This higher width of the humidifier makes it harder for the flow to take along all the produced water particles. Also, this flow has a higher

capacity and thus combining those two differences causes a low laminar flow to leave most of the produced water particles inside of the humidifier. But when the flow increases and therefore becomes more turbulent, the amount of water particles the flow carries increases. For the top and bottom humidifiers it seems that the flow already carries along all the produced water particles. Therefore, an increase in set velocity means an increase in the total amount of volume that needs to be supplied with water droplets per unit of time. Hence an increase of the set humidity is needed to keep a constant data rate.
During this measurement is the set humidity in the middle channel humidifier hold fixed at 11%, while the set humidity in the top/bot channel humidifiers is also hold fixed at 40%. The reason why the set humidity in the top/bot channel humidifiers is also hold fixed, comes from the unstable data rate at lower set humidity values.

4.2 Velocity profile compared with simulation (0.2 m/s)

In this section, the velocity profile is shown for a flow with a set velocity of $0.2\ m \cdot s^{-1}$. The velocity profile is also compared to a simulation, which is made with MATLAB. This simulation is based on a fully developed, rectangular flow, where the mean velocity can be set manually. The profile of the flow is measured along the $z - axis$ at $x = 1500\ mm$. The flow profile is measured two times, because during the first measurement, the humidifiers became too hot and stopped working. During the second measurement, ice was added to the humidifier feed water, which kept the humidifier working at a lower temperature. The velocity profiles and the theoretical velocity profile are shown in figure 15.

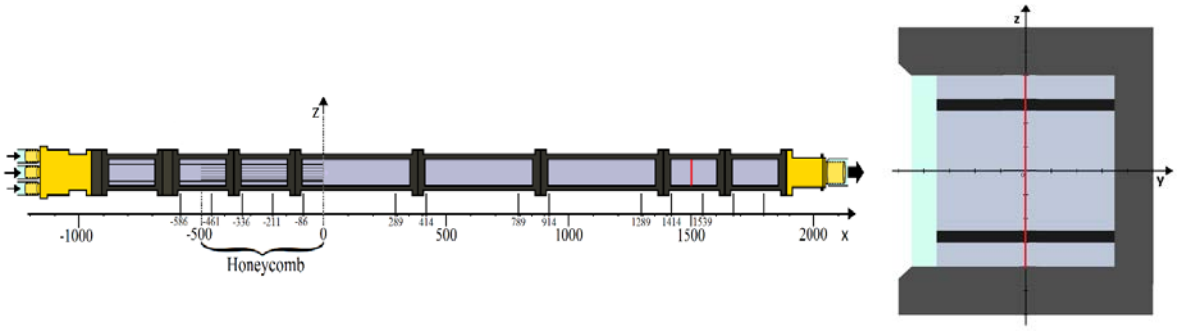

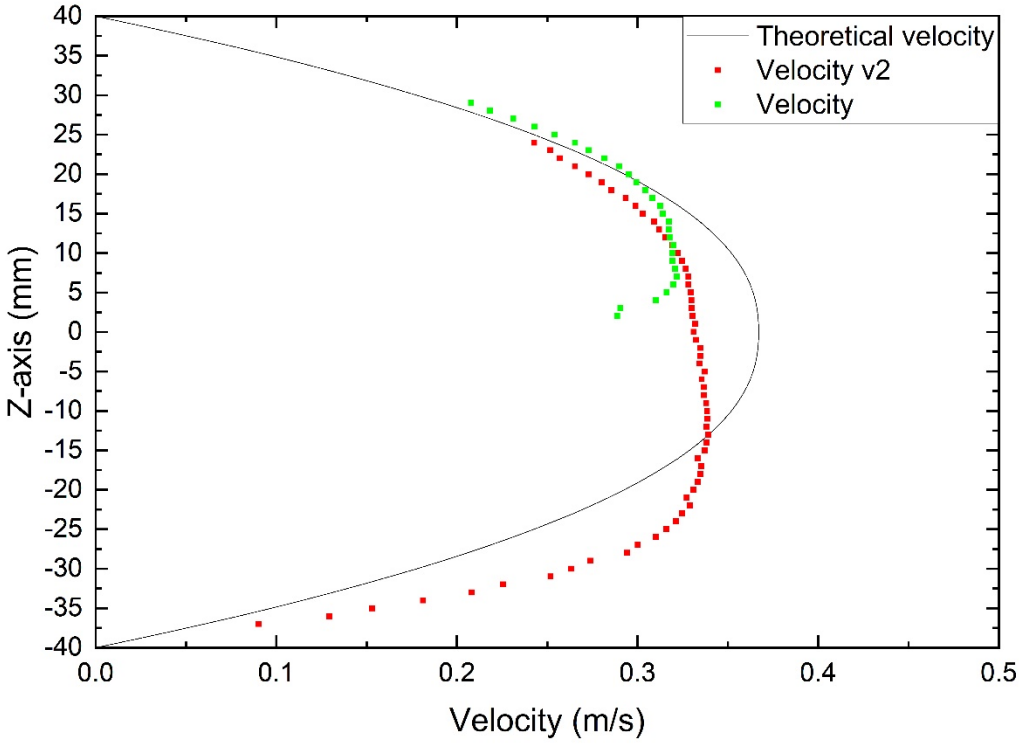

Figure 15 : Velocity profile with $v_{set} = 0.2$ m/s measured 1500 mm behind honeycomb along the Z-axis.

The cross sectional flow area upstream of the honeycomb is $4900\ mm^2$, while the area downstream is $5600\ mm^2$. This is a factor $\frac{7}{8}$, which means that the mean velocity, and so the MATLAB velocity are a factor $\frac{7}{8}$ of the set velocity, which is $0.175\ m \cdot s^{-1}$.
It can be seen that both profiles have a lower maximum velocity than the theoretical values. The experimental profile also has a more flattened character, while the Reynolds number with this velocity is only $Re = 865$. This is in the laminar regime, which means that the velocity profile has to become parabolic further downstream. This can be confirmed, when looking at the laminar entrance length, which is $L_{h,lam} = 3229\ mm$. This means that the flow is not even close to its laminar entrance length, which explains its flattened shape.

4.3 Velocity profile compared with different simulation velocities (0.1 m/s)

In section 4.2, with a v_{set} of $0.2\ m \cdot s^{-1}$, the laminar velocity profile was not yet visible due to the long entrance length. To check if there is still a laminar flow profile possible at the end of the wind tunnel, the same measurement as in section 4.2 is done, but now with a v_{set} of $0.1\ m \cdot s^{-1}$.
There is a problem however, it is known that the upper and lower channel cannot create a v_{set} of below $0.2\ m \cdot s^{-1}$, which means that only the middle channel can create a flow at this low velocity. The velocity profile is measured along the $z - axis$ at a distance of $1500\ mm$ behind the honeycomb. This velocity profile is also measured two times, because of the overheating of the humidifier. The velocity profiles with the theoretical profiles are shown in figure 16.

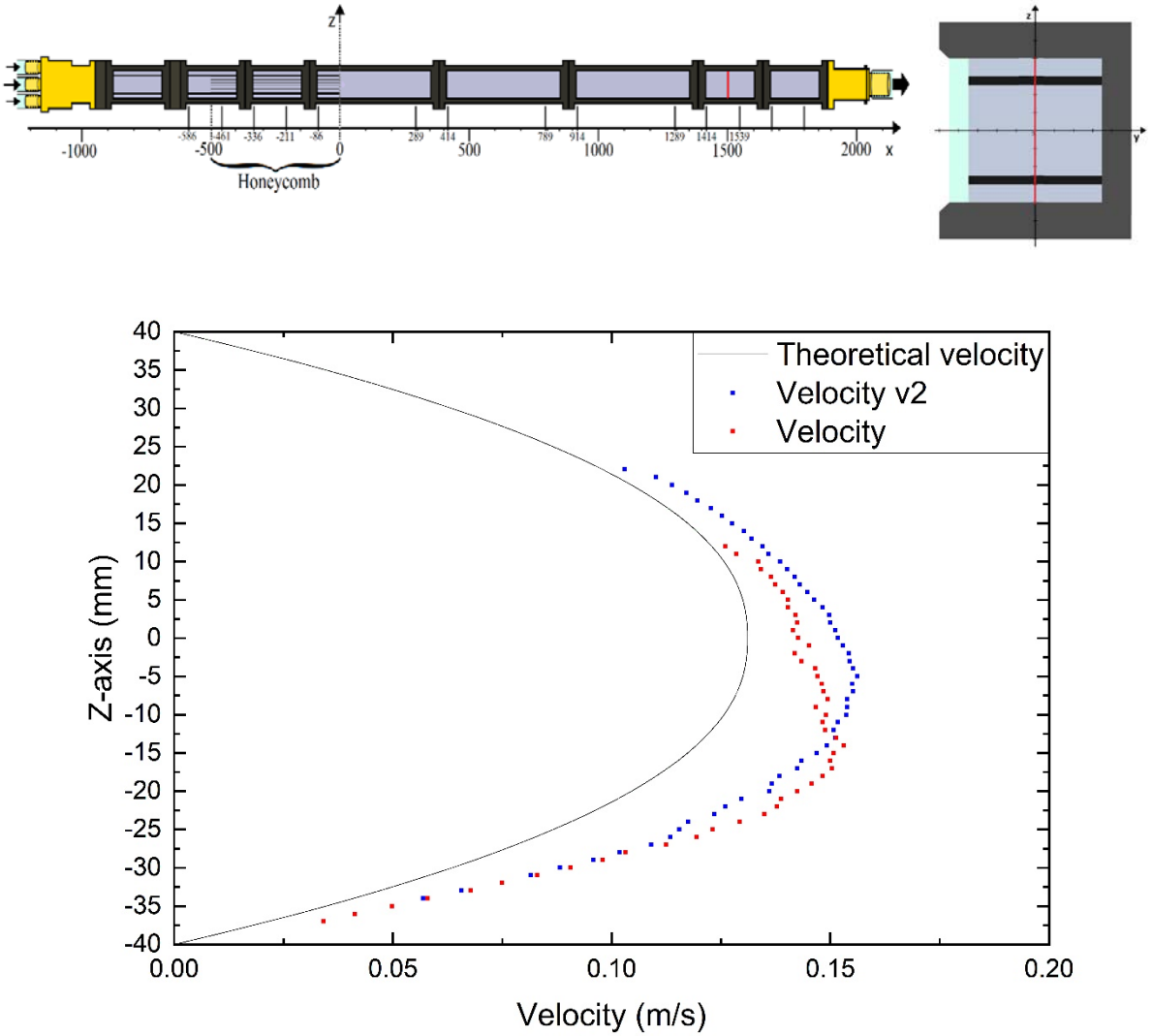

Figure 16 : Velocity profile with $v_{set} = 0.1$ m/s measured 1500 mm behind honeycomb along Z-axis.

The black graph shows the theoretical values with a $v_{set} = 0.1\ m \cdot s^{-1}$, where the velocity is only set in the middle channel. The blue points indicate the measurement that has been done without the stops. It can be seen that the experimental values are now higher than the theoretical values. The reason for this still has to be determined.
The cross sectional flow area upstream of the honeycomb is now $3500\ mm^2$, while the area downstream is $5600\ mm^2$. This means that the mean velocity at $x = 1500\ mm$, and so the MATLAB velocity, is a factor $\frac{5}{8}$ of the set velocity, which is $0.0625\ m \cdot s^{-1}$.
It can be seen that the velocity profile looks parabolic, which is an indication of a laminar-like flow. The Reynolds number for this velocity is $Re = 432$, which indeed corresponds to a laminar flow pattern. The entrance length at this Reynolds number is $L_{h,lam} = 1613\ mm$, which means that the flow is close to being fully-developed. This also explains the parabolic flow profile.
The experimental value at $z = 0\ mm$ is $16\ \%$ higher than the theoretical value at the same point. This difference is substantial and cannot be neglected. Because of this difference, the velocity profile along the y axis at $z = 0\ mm$ has also been measured at $x = 1500\ mm$ and is compared with the profile along the $z - axis$, which is shown in figure 17.

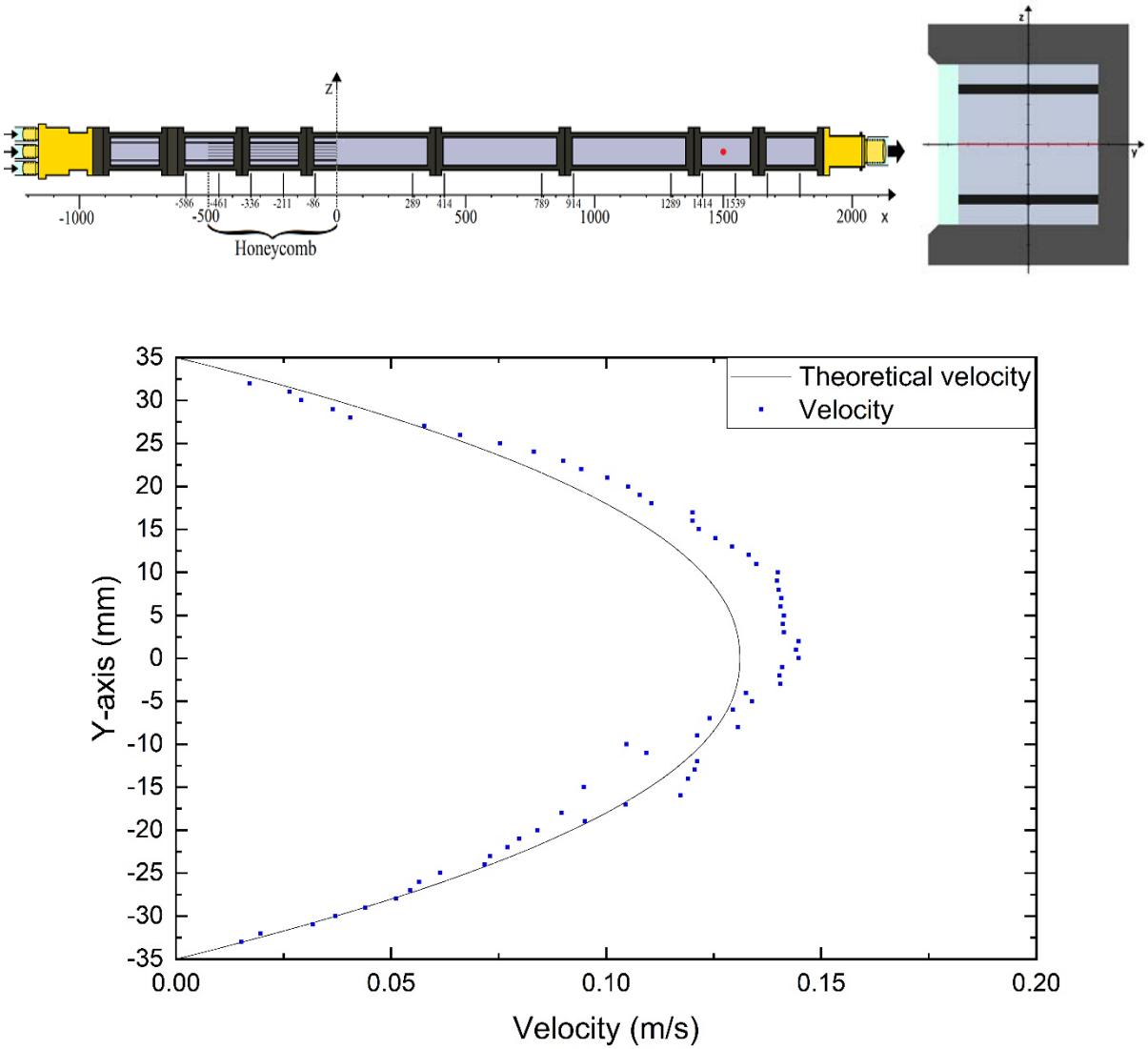

Figure 17 : Velocity profile with $v_{set} = 0.1$ m/s measured 1500 mm behind honeycomb along Y-axis.

This profile is similar to the profile along the $z - axis$, which was also expected due to the almost rectangular shape of the wind tunnel. In figure 17 can be seen that the experimental values are still higher than the theoretical values. The velocity at $y = 0\ mm$ should be equal to the velocity at point $z = 0\ mm$, because that is the only point where the two velocity profiles overlap. The velocities at those points are: $v_{z=0} = 0.152\ m \cdot s^{-1}$ and $v_{y=0} = 0.145\ m \cdot s^{-1}$, which is a difference of 5%. This difference is substantial. The reason for this difference is the noise, which affects each measurement and makes sure that two identical measurements can never have the same output.
When different mean velocities are put into the MATLAB script, the mean velocity of $0.075\ m \cdot s^{-1}$ looks the most like the blue-dotted flow pattern of figure 16. This mean velocity of $0.075\ m \cdot s^{-1}$ is $20\ \%$ higher than what the mean velocity should be, which is $0.0625\ m \cdot s^{-1}$. The comparison between those two flow patterns is shown in figure 18.

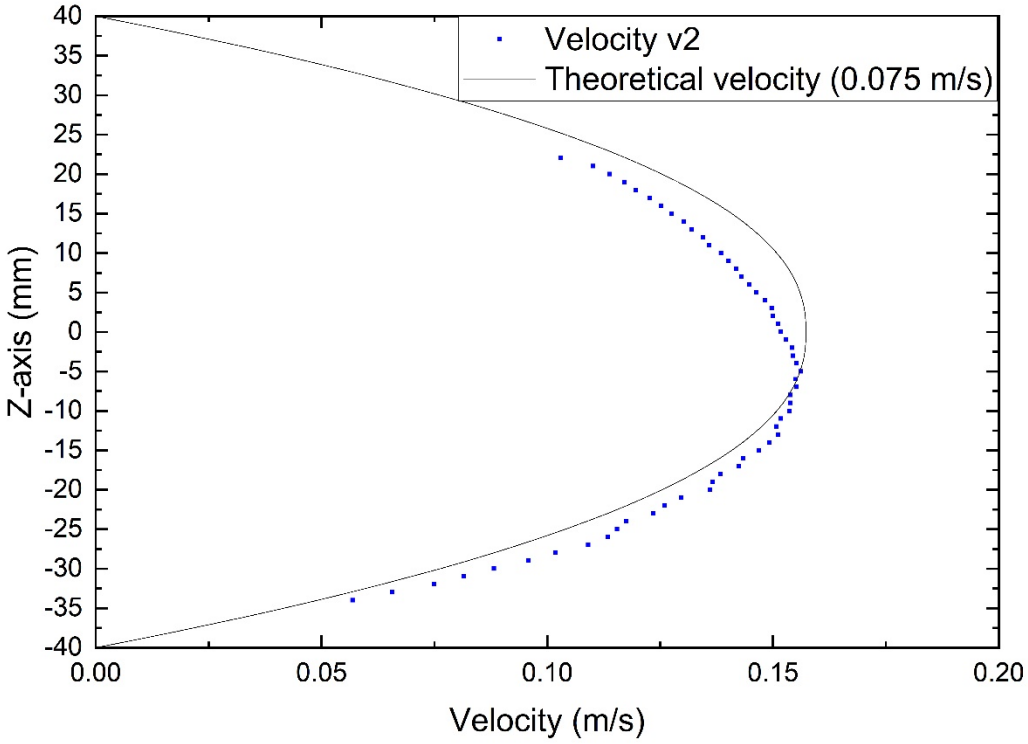

Figure 18 : Velocity profile along Z-axis compared with 0.075 m/s simulation velocity flow profile 1500 mm behind honeycomb.

It can be seen that the velocity profile is still not the same as the theoretical velocity profile with $v_{mean} = 0.075\ m \cdot s^{-1}$. First of all, the top of the flow parabola is not at $z = 0\ mm$, but $7\ mm$ below. The reason for this is probably gravity; water droplets inside the flow experience a gravitational force which is directed downward, which means that they are not measured at $z = 0\ mm$, but a bit lower.
In this paragraph can be seen that every measurement value has a significant difference $(15 - 20\%)$ compared to its MATLAB value. These differences are probably due to a combination of valve control errors plus small offset errors in LDV equipment.

4.4.1 Turbulence intensity measurement in the transition region

This part of the results shows the turbulence intensity of the flow at different velocities inside the wind tunnel. The measurements are taken in the Reynolds region where the transition from a laminar flow to a turbulent flow takes place. In research before, the turbulence intensity was measured for a broad range of Reynolds numbers, but there were never detailed measurements in the transition region itself. The measurements were taken $5\ mm$ behind the honeycomb in the

middle of the wind tunnel, which means that the flow pattern can be considered the same as in a channel at the end of the honeycomb.

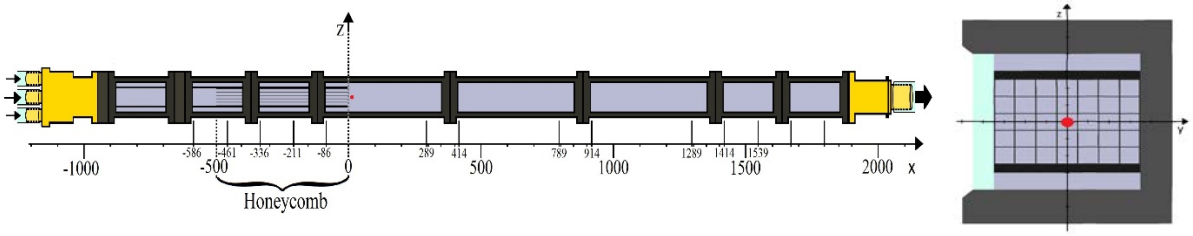

The values of the turbulent intensity are measured for the set velocities ranging from $2.0 - 3.5\ m \cdot s^{-1}$, with steps of $0.1\ m \cdot s^{-1}$, in increasing and decreasing order. To give a clear indication at which Reynolds numbers the transition from a laminar to a more turbulent flow takes place, the set velocities are converted into the corresponding Reynolds numbers. Despite the fact that the measurements took place $5\ mm$ behind the honeycomb, the Reynolds numbers are based on the hydraulic diameter of the honeycomb channels. The turbulence intensity is measured as a function of increasing and decreasing velocities, which can be seen in figure 19.

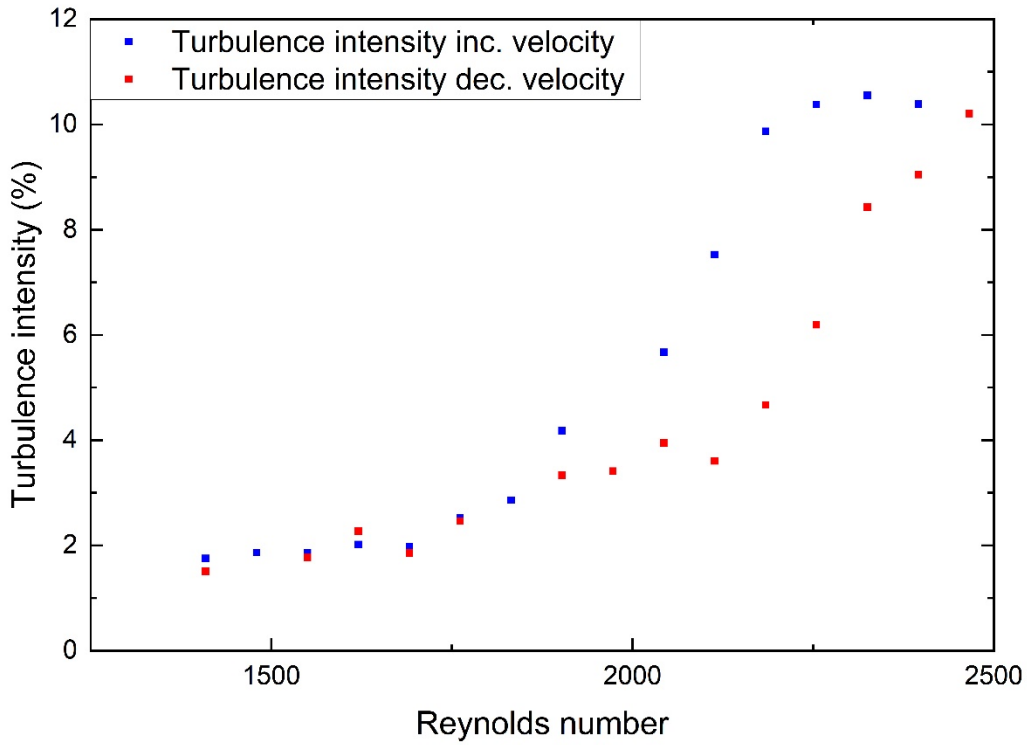

Figure 19 : Turbulence intensity as a function of Reynolds number.

It can be seen that the profile of the turbulence intensity as a function of increasing Reynolds numbers differs from the profile with decreasing Reynolds numbers. At increasing velocities, the turbulence intensity starts to increase at lower Reynolds numbers, compared to the profile with decreasing velocities. The peak of the turbulence intensity at increasing velocities also occurs at a lower Reynolds number, compared to the turbulence intensity peak of the decreasing velocities.
In the rest of this research, the turbulence intensity profile of the increasing velocity is used, because during measurements, the velocity goes from a low to a higher value.
The transition from a laminar to a turbulent flow starts around $Re = 1750$, where the turbulence intensity starts increasing. It cannot be said at which Reynolds number there is self-sustaining turbulence, because there is not enough data at higher Reynolds numbers. At $Re = 2300$, the

turbulence intensity has a peak value around 11%. This peak value tends to decrease at $Re > 2300$. This means that the transition region starts at $Re = 1750$ and ends at $Re > 2300$. This is not completely in agreement with the theoretical values for the transition Reynolds numbers, which state that the flow is laminar for $Re < 2300$ and that the transition from a laminar to a turbulent flow takes place between $2300 < Re < 4000$. Factors which could influence this difference are the assumptions that the flow inside a honeycomb channel is a square duct- flow, while the values from the literature are based on a circular pipe flow. Another cause for the difference could be the assumption that the velocity profile $5\ mm$ behind the honeycomb is exactly the same as the profile at the end of a honeycomb channel, which is of course, not completely the case.

4.4.2 Comparison with paper

This part contains a comparison between data measured in section 4.4.1 and the data from Owolabi et al. (2016) [1]. This means that the measurements were taken $5\ mm$ behind the honeycomb in the middle of the wind tunnel and that flow pattern can be considered the same as in a channel at the end of the honeycomb. In the paper from Owolabi et al., the measurements were taken in the middle of an empty, rectangular wind tunnel, with a fully-developed laminar flow.
This comparison will be made clear with the use of graphs where the turbulence intensity and the mean stream wise velocities $< U >$ normalized by the bulk velocity U_b are measured as a function of the Reynolds number. Both relations between the turbulence intensity and the Reynolds number are shown in figure 20.

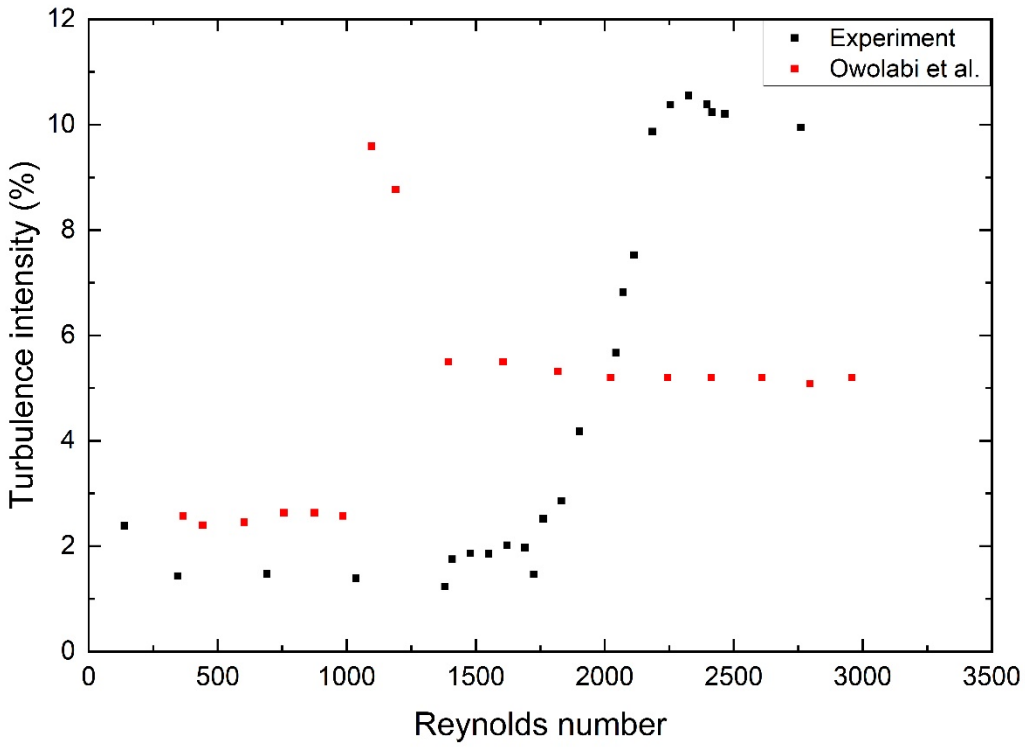

Figure 20 : Turbulence intensity as a function of the Reynolds number [1].

It can be seen that the turbulence intensities from Owolabi et al. (red dots) remain constant at a value of $\pm 2.5\ \%$ up to a Reynolds number of $Re = 1000$. This means that the flow can be considered laminar at $Re \leq 1000$. In the range from $1000 < Re < 1400$, the turbulence intensity goes up and down with a peak value of $9.6\ \%$ at $Re = 1100$. The flow is in transition from a laminar profile to a more turbulent profile in this range. From $Re > 1400$, the turbulence intensity remains

almost constant with a value of $\pm 5.5\ \%$, which means that the flow has self-sustaining turbulence at $Re \geq 1400$.
The turbulence intensity profile of this research (black dots) is almost the same profile as the blue dotted profile in section 4.4.1, but some values were added from research of a previous student, K. Kuiper [18]. These extra values were added to get a broader range of Reynolds numbers. The Reynolds numbers corresponding to the different flow regimes are the same as in section 4.4.1. While the two profiles differ a lot, there are also some similarities; both profiles have a constant turbulence intensity up to a certain Reynolds number and they also have a region where the turbulence intensity has a peak value and then decreases.

Both values of $< U > / U_b$ can also be plotted as a function of the Reynolds number, which is done in figure 21 . The mean stream wise velocity $< U >$ is just the measured velocity at the middle of a honeycomb channel, and the U_b is the mean velocity inside a honeycomb channel.

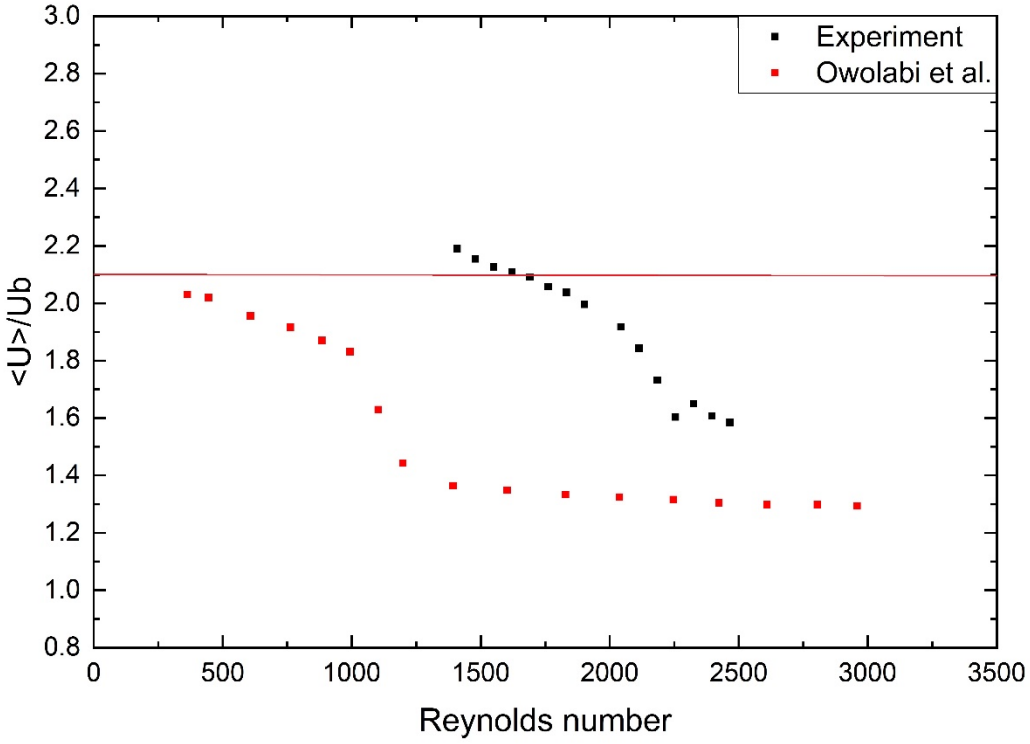

Figure 21 : <U>/Ub as a function of the Reynolds number [1].

According to the analytical solution of a fully-developed laminar flow, the value of $< U > / U_b$ should remain constant in the laminar flow regime ($Re \leq 1000$), which is indicated with the red line. The experimental data from the paper (red points) show that this is not the case. The reason for this is, according to the paper, the Coriolis force, which influences the flow in the laminar regime and causes the difference between the $< U > / U_b$ points and the red line up to $Re = 1000$. There is also a drop in the $< U > / U_b$ values between $1000 < Re < 1400$, which corresponds to the transition region between a laminar and turbulent flow. From $Re \geq 1400$, in the turbulent flow regime, the $< U > / U_b$ values remain constant again.
The $< U > / U_b$ values from this research should also have an almost constant value in the laminar flow regime, according to the analytical solution of a fully-developed laminar flow. This is not the case, because the values of $< U > / U_b$ do not have a constant value in the laminar regime ($Re \leq 1750$). This deviation from a constant value is also due to the Coriolis force. It can be seen that there

is a similar-like drop in the values of $< U >/U_b$ which starts at $Re = 1750$. The transition from a laminar to a turbulent flow profile also starts at $Re = 1750$.
From the data can be concluded that the deviation of the $< U >/U_b$ values from the analytical solution of a fully-developed laminar flow can be explained by the presence of the Coriolis force. Also can be concluded that the drop in the $< U >/U_b$ values is in the same Reynolds region as the transition region of a laminar to a turbulent flow. When the flow has become fully turbulent, the $< U >/U_b$ values remain constant again at a lower value than in the laminar case.

The reason why the $< U >/U_b$ values and the turbulent intensity values of this research differ from the values according to the paper, is unknown. It can be seen that the two profiles in both graphs have a similar-like shape, but that the experimental graph is shifted to the right, which means that the flow regimes are in a different range of Reynolds numbers.

4.5 Flow patterns at a set velocity of 2m/s

In this part, the velocity and RMS profiles at different locations inside the wind tunnel are shown for a set velocity of 2 m/s. The flow profiles along the $z - axis$ of the wind tunnel were measured $(5, 50, 100, 200, 500$ and $1000\ mm)$ behind the honeycomb. The different velocity profiles at those locations downstream the honeycomb are shown in figure 22.

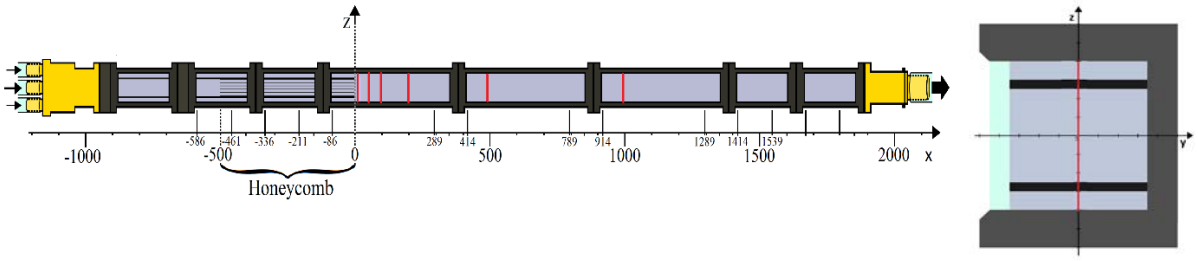

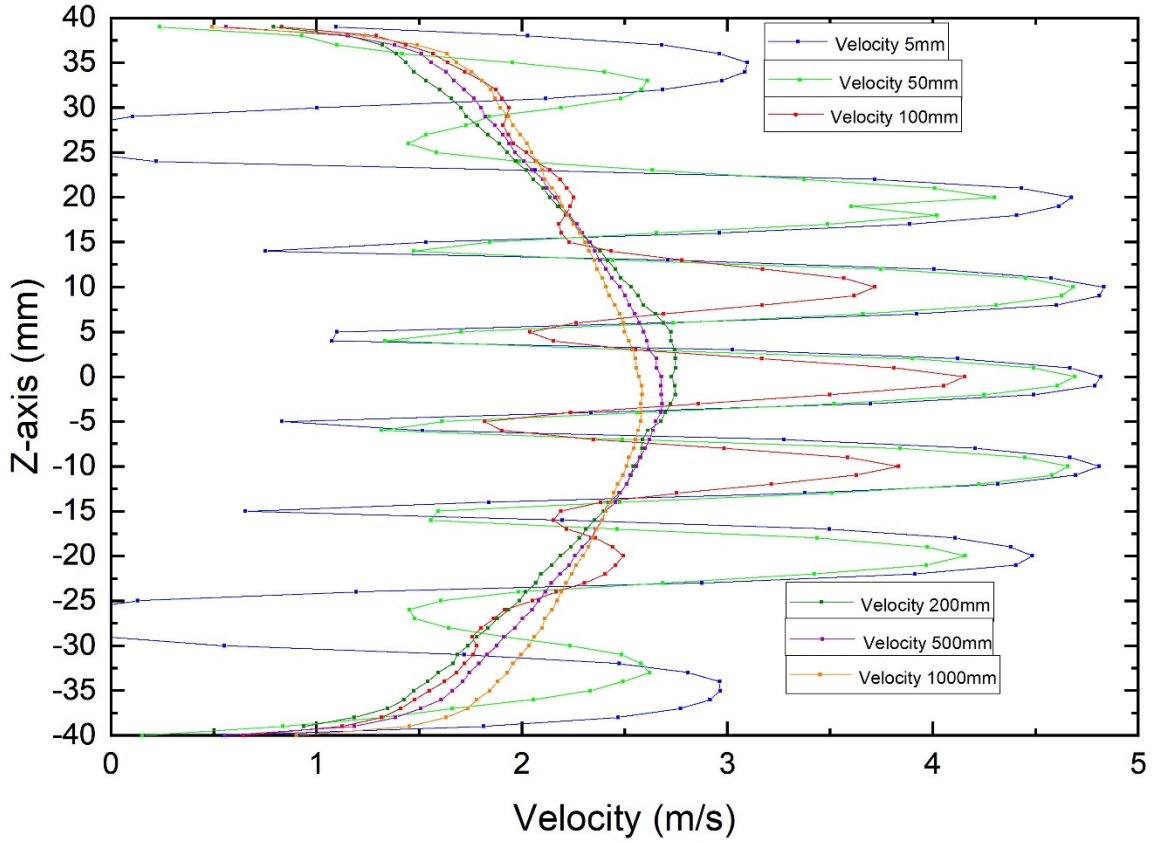

Figure 22 : Velocity profiles along the Z-axis at different locations behind the honeycomb.

Looking at the Reynolds number inside a honeycomb channel ($Re = 1401$) and in the channel downstream the honeycomb ($Re = 8649$) with a set velocity of $2\ m \cdot s^{-1}$, the behavior of the different flow profiles can be explained. Downstream of the honeycomb, vortex shedding occurs, which results in mixing.

The vortices, which are created by the channel separation walls, are also visible in the velocity profile $5\ mm$ behind they honeycomb; at the level of the separation walls at $-25\ mm$ and $+25\ mm$ are even negative velocities measured. Furthermore, the laminar profiles from the honeycomb channels are almost the same, because the mixing is not yet visible at $5\ mm$.

Further inside the wind tunnel has the effect of the mixing become visible; the parabolic profiles originating from the honeycomb channels are symmetrically damped out due to the mixing (50 and $100\ mm$) until they are no longer visible.

The parabolic profiles of the honeycomb channels are no longer visible in the velocity profiles $200, 500$ and $1000\ mm$ behind the honeycomb. Also can be seen that the profiles of $200, 500$ and $1000\ mm$ are getting a more fattened shape further downstream. This means that the profile should become turbulent in the end, because $Re = 8649$. Calculations show that the turbulent entrance length is $L_{h,turb} = 1488\ mm$, which means that the flow should be fully turbulent at the end of the wind tunnel.

To give a clear indication about what happens inside the wind tunnel, the RMS values at each distance downstream the honeycomb are shown below in figure 23.

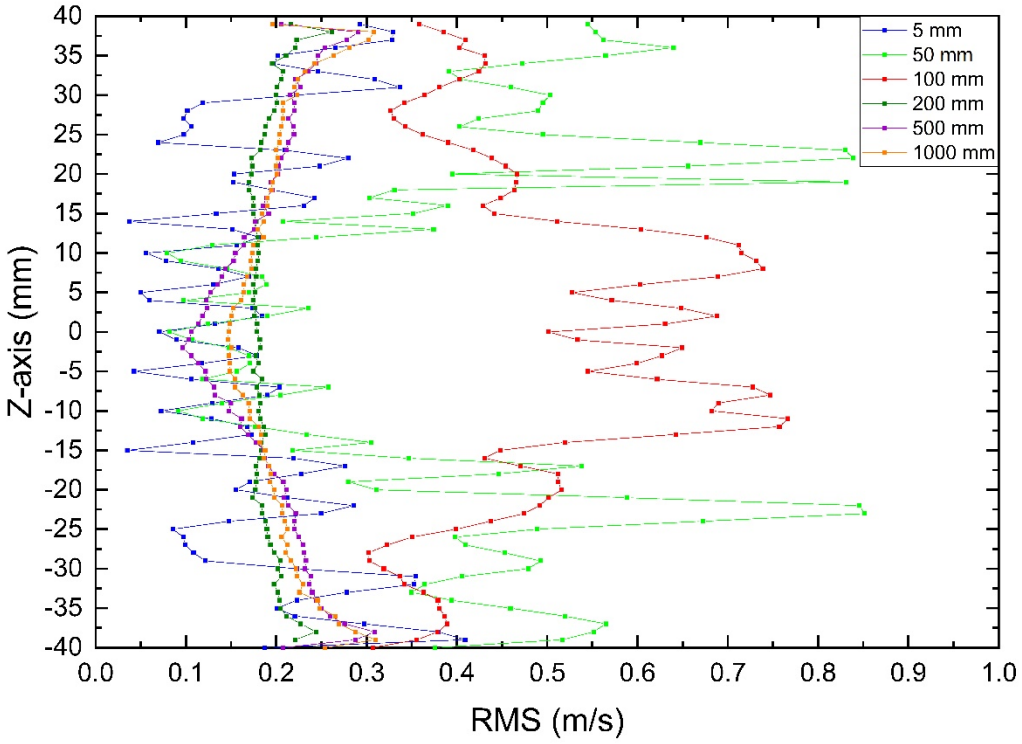

Figure 23 : RMS *profiles along the Z axis at different locations behind the honeycomb.*

At $5\ mm$ downstream the honeycomb, the RMS values are low and they have a saw like shape. This saw like shape originates from the honeycomb cells. The RMS values are the lowest at the places where the walls of the honeycomb cells are. Looking at the RMS profile $50\ mm$ downstream the honeycomb, can be seen that the mixing process has already started. There are two RMS peaks which coincide with the two channel separation walls. The RMS profile between those two peaks is almost the same as the $5\ mm$ profile, which is also the case in the velocity profiles.
For the $100\ mm$ profile, the overall RMS values are relatively high, but the sharp RMS peaks are damped out at the top and bottom of the wind tunnel. Between the heights 15 and $-15\ mm$ is the saw shaped structure of the RMS still visible, but with higher values than at 5 and $50\ mm$.
The profiles of $200, 500$ and $1000\ mm$ are almost the same and almost have the same RMS values along the $z - axis$.

5. Conclusion and discussion

Conclusion

Looking at the results from chapter 4, different conclusions can be made according to the data. The first conclusion that can be made is that the minimal set humidity of a humidifier in the top or bottom channel is only a function of the set velocities in those channels. The minimal set humidity of the middle humidifier is independent from the set velocity in the middle channel, because it remains constant at different set velocity values.
Also can be concluded that the flow profile with a $v_{set} = 2.0\ m \cdot s^{-1}$ $(Re = 865)$ is not yet fully developed at the end of the wind tunnel, because the entrance length at this Reynolds number is $L_{h,lam} = 3229\ mm$, which explains its flattened shape.
At $v_{set} = 0.1\ m \cdot s^{-1}$, with $Re = 432$, the flow profile is laminar and has the characteristic parabolic shape at the end of the wind tunnel. This is in agreement with the calculations, because the entrance length at this Reynolds number is $L_{h,lam} = 1613\ mm$, which means that the flow is almost fully developed. However, the difference between the experimental and the theoretical flow profile is almost 16%, which is significant.
According to section 4.4.1, the transition from a laminar to a more turbulent regime inside a honeycomb cell starts around $Re = 1750$, which is not in agreement with the value according to the literature [5].
Section 4.4.2 shows that in the transition regime between a laminar and turbulent flow, a drop in the $< U > / U_b$ values can be seen. This is also what is expected, because $< U >$ is lower in a turbulent like flow compared to a laminar flow; when the flow profile becomes more flattened, which is the case in the transition regime, the mean velocity , $< U >$, goes down in the middle.
The reason why the $< U > / U_b$ values differ from the analytical solution of a fully-developed laminar flow in the laminar regime can be explained by the Coriolis force. This is also explained in the paper written by Owolabi et al. [1], but the data from this research confirms this. The laminar regimes of the paper and this research are $Re \leq 1000$ and $Re \leq 1750$, which means that there is a significant difference between those number, which cannot be explained.
According to the last section, 4.5, can be concluded that the effect of the honeycomb cells and the separation walls become less visible further inside the wind tunnel, due to the mixing that takes place. Also can be concluded that the flow profiles almost remain the same after the laminar honeycomb profiles are damped out.

Discussion

During this research, many factors could be responsible for the differences between the experimentally gathered results and the results according to the theory.
First of all is gravity, due to gravity, the water droplets are moving downwards. This creates a measured flow profile which is shifted to the bottom of the wind tunnel. The effect of gravity on the flow occurs at lower velocities ($v_{set} \leq 0.2\ m \cdot s^{-1}$).
The second and most important, is the systematic measurement error, which is largely responsible for the $15 - 20\%$ measurement differences between the theoretical and experimental values. This error comes probably from the combination of valve control errors plus small offset errors in the LDV equipment.
At last are the assumptions, which are assumed to be constant, but vary in the real world. The viscosity is assumed to be constant during this research, which means that the viscosity is assumed to have no temperature dependence. This is not the case, and this differs the Reynolds number: when taken the viscosity temperature dependence into account, the Reynolds number would differ up to a maximum of $2.1\ \%$ from the temperature independent solution. These values are calculated with a lab temperature which is between 20 and $28\ °C$**.** During this research the viscosity of nitrogen is used with a temperature of $20\ °C$**.**

Suggestions for further research

For further research, it would be interesting to measure the flow profiles at different x coordinates along the $z - axis$ at higher velocities inside the wind tunnel. It would be interesting to know what the effect of the mixing process is at higher velocities. Measuring at higher velocities was not possible during this research, because there was not enough time left.
It could also be important to find out which errors are responsible for the $15 - 20\%$ difference between theoretical and experimental values. This is a lot of work, because it is not exactly known which error or errors are responsible for these differences.
At last, it would be important to do measurements with different types of honeycombs. It was also the idea that this was done during this research, but this was also not possible due to time issues. Measurements can also be done with honeycombs with different dimensions or honeycombs with different geometries; during this research is an almost squared honeycomb channel used, but the flow properties (hydraulic diameter) would change when the channels have different geometries. Other types of honeycombs can be found in the appendix.

Acknowledgements

I am very thankful that I had the chance to do my Bachelor End Project with the help of The Turbulence and Vortex Dynamics group. I really enjoyed my time and I want to thank the people that helped me during my project.

First of all, I want to thank my supervisor Rik Dellaert. He helped me to get used to the setup, so that I could perform measurements on my own. He has also been a nice and patient person if I had some trouble during the measurements, which gave me a good feeling. I also want to thank him for the multiple times that he gave me feedback on my report, because I had some trouble writing it.

Next, I want to thank Jos Zeegers, the project leader. Also, for his feedback on the report, which was very specific and detailed. It was also nice to discuss some results with Jos, because he has the knowledge to really explain the flow profiles and he gave me some extra background information about the subject.

Finally, I want to thank Jorgen van der Veen, for teaching me the about the dangers of the lasers and the technical support.

Bibliography

[1] D. J. C. Owolabi, Bayode E., Poole, Robert J., Dennis, “Experiments on low-Reynolds-number turbulent flow through a square duct,” 2016.

[2] Greenpreace, “Toxic exosystems: The Impact of Plastic on Marine life.”

[3] Sarah Gibbens, “Plastic proliferates at the bottom of world’s deepest ocean trench.” [Online]. Available: https://news.nationalgeographic.com/2018/05/plastic-bag-mariana-trench-pollution-science-spd/.

[4] Radboud University, “STW grant: recycling high-tech materials with magnetic density separation.” [Online]. Available: https://www.ru.nl/hfml/news/news/news-items/stw/.

[5] “Reynolds number.” [Online]. Available: http://www.valvias.com/reynolds-number.php.

[6] C. J. Seeton, “No Title,” *Viscosity-temperature correlation for liquids*, 2006. .

[7] “Gases-Densities.” [Online]. Available: https://www.engineeringtoolbox.com/gas-density-d_158.html.

[8] “Gases-Dynamic Viscosity.” [Online]. Available: https://www.engineeringtoolbox.com/gases-absolute-dynamic-viscosity-d_1888.html.

[9] “Entrance length.” [Online]. Available: https://en.wikipedia.org/wiki/Entrance_length.

[10] I. S. Technico, “Transition from Laminar to Turbulent Flow.” [Online]. Available: https://fenix.tecnico.ulisboa.pt/downloadFile/3779576279970/Class6.pdf.

[11] “Laminar, Transitional or Turbulent Flow,” 2004. [Online]. Available: https://www.engineeringtoolbox.com/laminar-transitional-turbulent-flow-d_577.html.

[12] “Turbulence intensity.” [Online]. Available: https://www.cfd-online.com/Wiki/Turbulence_intensity.

[13] A. Vujinovic, “Kelvin-Helmholtz Instability,” 2015.

[14] E. Imster, “Clouds that look like ocean waves.” [Online]. Available: https://earthsky.org/earth/kelvin-helmholzt-clouds.

[15] “Karman vortex street.” [Online]. Available: https://en.wikipedia.org/wiki/Kármán_vortex_street.

[16] Dantec Dynamics, “Measurement principles of LDA.” [Online]. Available: https://www.dantecdynamics.com/measurement-principles-of-lda.

[17] I. Bruining, “Decay of wake turbulence generated by honeycombs for magnetic density separation,” TU/e.

[18] K. Kuiper, “The wake of a honeycomb applied in a magnetic density separator.”

Appendix

Honeycombs

Name	Measures: Outside: Length (y-axis) [mm]	±	Width (x-axis) [mm]	±	Height (z-axis) [mm]	±	inside: Wall thickness [mm]	Cell-width (x-axis) [mm]	Cell-height (z-axis) [mm]	Number of cells: x	z	tot	Calculated properties: Hydraulic diameter [mm]	Solidity
HC10Mc	100	1	69,7	0,1	49,4	0,1	3,2	6,3	6,4	7	5	35	6,35	0,590
HC20Mc	200	1	69,7	0,1	49,4	0,1	3,2	6,3	6,4	7	5	35	6,35	0,590
HC30Mc	300	1	69,7	0,1	49,4	0,1	3,2	6,3	6,4	7	5	35	6,35	0,590
HC10Gc1	100	1	69,7	0,1	49,4	0,1	0,4	9,5	9,4	7	5	35	9,45	0,092
HC20Gc2	100	1	69,7	0,1	49,4	0,1	0,4	9,5	9,4	7	5	35	9,45	0,092
HC25Gc	250	1	69,7	0,1	49,4	0,1	0,4	9,5	9,4	7	5	35	9,45	0,092
HC50Gc	500	1	69,7	0,1	49,4	0,1	0,4	9,5	9,4	7	5	35	9,45	0,092
HC20Sc	200	1	69,7	0,1	49,4	0,1	1	1,987	2,025	16	16	256	2,01	0,701

Ends

	Measures: Outside: Length (y-axis) [mm]	±	Width (x-axis) [mm]	±	Height (z-axis) [mm]	±	inside: Wall thickness [mm]	Cell-width (x-axis) [mm]	Cell-height (z-axis) [mm]	Type	Point length [mm]	Tip size [mm]	Angle [degrees]
EHCf00Mc	50	1	69,7	0,1	49,4	0,1	3,2	6,3	6,4	Flat	-------	-------	-------
EHCp03Mc	50	1	69,7	0,1	49,4	0,1	3,2	6,3	6,4	Pointed	3	0,2	26,57
EHCp06Mc	50	1	69,7	0,1	49,4	0,1	3,2	6,3	6,4	Pointed	6	0,2	14,04
EHCp20Mc	50	1	69,7	0,1	49,4	0,1	3,2	6,3	6,4	Pointed	20	0,2	4,29

Figure 24 : Overview of all the different types of honeycombs with their specifications